

Genome Mining and Heterologous Expression-Guided Discovery of Mangicol Sesterterpenoids with Antimicrobial and Antineuroinflammatory Activities

Cuiping Xing, Huanting Yang, Kangjie Lv, Keying Lan, Guoliang Zhu, Bin Zhu, Biao Ren, Yi Jiang, Chenglin Jiang, Huanqin Dai, Xuming Mo, Tom Hsiang, Wael M. Abdelmageed, Lixin Zhang, Lan Jiang,* and Xueting Liu*



Cite This: *J. Agric. Food Chem.* 2025, 73, 19474–19483



Read Online

ACCESS |



Metrics & More



Article Recommendations



Supporting Information

ABSTRACT: The accelerating increase in antimicrobial resistance presents serious dangers to global health, food safety, and agricultural productivity. In this study, we explored fungal-derived sesterterpenoids as potential antimicrobial agents, focusing on mangicols biosynthesized by a newly identified bifunctional terpene synthase from *Fusarium oxysporum* 14005. By combination of genome mining, heterologous pathway reconstitution, and feature-based molecular networking, eight new mangicols featuring epoxy and tetrahydrofuran moieties on their side chains were identified and characterized. Antimicrobial assays revealed that several of these derivatives exhibited potent activity against *Ralstonia solanacearum*, *Staphylococcus aureus*, and *Streptococcus mutans*, with minimum inhibitory concentrations ranging from 6.25 to 25 μ M. Furthermore, compounds 3–5 demonstrated significant antineuroinflammatory effects in murine BV2 microglial cells with 50.0, 53.13, and 48.05%, respectively. The results offer mechanistic insights into the biosynthesis and bioactivity of mangicol-type sesterterpenoids and support their potential as novel antimicrobial and anti-inflammatory agents for addressing antimicrobial resistance.

KEYWORDS: phytopathogenic fungus, sesterterpenoid, heterologous expression, mangicol, FBMN, antibacterial activity, antineuroinflammatory

INTRODUCTION

The rapid emergence of antimicrobial resistance (AMR) has become a pressing global challenge, with profound implications for human health, food safety, and agriculture.^{1–3} Antimicrobial-resistant pathogens pose significant challenges to both human health and food security. In the context of food safety, while both drug-sensitive and drug-resistant bacteria are capable of triggering outbreaks, infections caused by resistant strains pose greater clinical challenges due to limited treatment options.⁴ Similarly, in agriculture, the extensive and sustained use of antimicrobial agents has led to the emergence and widespread dissemination of resistant bacterial populations, thereby compromising the efficacy of standard antimicrobial therapies and threatening both crop productivity and animal health.⁵ Particularly alarming is the global prevalence of certain pathogenic species, including *Staphylococcus aureus* (*S. aureus*), a major contributor to foodborne disease outbreaks,^{6,7} and *Ralstonia solanacearum* (*R. solanacearum*), a highly destructive phytopathogen known to infect over 200 plant species, including economically vital crops like tomatoes, bananas, and potatoes.^{8,9} The escalating burden of AMR underscores the urgent need for novel antimicrobial agents. Fungi represent an invaluable reservoir of bioactive natural products, with terpenoids emerging as one of the most diverse and pharmacologically significant classes of compounds.^{10–13} Fungi-derived terpenoids, including mangicols,¹⁴ ophiobolin,¹⁵ and fusidic acid,¹⁶ possess diverse activities, such as anti-

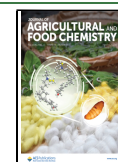
inflammatory, antimicrobial, and anticancer. Notably, in bacterial and plant terpenoid biosynthetic gene clusters, prenyltransferase (PT) and terpene cyclase (TC) generally exist independently.¹⁷ In contrast, filamentous fungi possess bifunctional terpene synthases (BFTSPs) that harbor a TC domain at the N-terminus and a PT domain at the C-terminus, exhibiting both prenyltransferase and terpene cyclase activities. The discovery of BFTSPs has further expanded the chemical space of terpenoid biosynthesis.¹⁸ Advances in genomic mining and heterologous expression techniques have facilitated the identification and characterization of numerous new diterpenoid and sesterterpenoid scaffolds, offering promising avenues for drug discovery.^{14,19,20} However, despite these advances, challenges remain in optimizing the biosynthetic yields of bioactive derivatives, often limiting their practical applications under standard laboratory conditions. Consequently, many potentially valuable fungal metabolites remain underexplored. To address these challenges, feature-based molecular networking (FBMN) has emerged as a powerful analytical approach for the rapid screening of structurally related compounds within

Received: April 3, 2025

Revised: July 15, 2025

Accepted: July 15, 2025

Published: July 24, 2025



complex mixtures.²¹ By integration of retention time, isotope patterns, and precursor ion data, FBMN improves isomer resolution and quantification, facilitating the discovery of bioactive terpenoids that might otherwise remain undetected.

During our investigation into bioactive fungal terpenoids,^{22,23} a biosynthetic gene cluster responsible for mangicol-type sesterterpenoid production was discovered within our fungal genome database. The purpose of this work was to use genome mining, heterologous expression, and FBMN-based metabolite profiling to discover new mangicols. We report the purification, structure determination, biological evaluation, and proposed biosynthetic pathways of these compounds. Our findings demonstrated the efficacy of combining FBMN with heterologous expression systems to systematically explore fungal terpenoid scaffolds. This integrated approach not only enhanced the discovery and characterization of novel bioactive derivatives but also provided robust theoretical and experimental frameworks for accelerating natural product research. Ultimately, these findings will contribute to the broader search for new antimicrobial agents, addressing the urgent need for alternative therapeutic strategies in the fight against AMR and emerging health threats.

MATERIALS AND METHODS

General Experimental Procedures. General experimental instruments and procedures employed in this work were consistent with those documented earlier.^{22,23}

Strains, Media, and Growth Conditions. *Fusarium oxysporum* (F. *oxysporum*) 14005 (CGMCC 21067), originally isolated from tomato, in Guangdong, China, was cultured on 2% PDA at 28 °C for 5 days for gene cloning. Heterologous expression was performed in *Aspergillus oryzae* (A. *oryzae*) NSAR1 (*niaD*[−]*sC*[−]*adeA*[−]Δ*argB::adeA*[−]),²⁴ which was grown in DPY broth. The transformants were cultured in an MPY broth. The detailed compositions and cultivation procedures for both media were described in our previous reports.^{22,23} *Escherichia coli* DH10B was used for cloning.

Genomic DNA Isolation and Plasmid Construction. Genomic DNA of *F. oxysporum* 14005 was extracted following the previously reported method.²² The *fomdA–F* genes (Table S1) were amplified using Q5 High-Fidelity Polymerase (NEB), with the genomic DNA serving as the template. The PCR products were cloned into pUARA4 or pUSA4 via a ClonExpress II OneStep Cloning Kit (Vazyme Biotech), and the constructed plasmids are listed in Table S2.

Transformation of A. oryzae. Protoplast transformation of *A. oryzae* NSAR1 (1.0 × 10⁷ cells) was performed using the protoplast-polyethylene glycol method,²⁵ resulting in the following transformants: AO-*fomdF* (pUSA4-*fomdF*), AO-*fomd* (pUARA4-*fomdABF* and pUSA4-*fomdCDEG*), and AO-control, as shown in Table S3. AO-*fomdF* and AO-*fomd* refer to *A. oryzae* transformants harboring the *fomdF* gene or the whole gene cluster (*fomdA–fomdG*), respectively. AO-control refers to the transformant harboring vector plasmids and used as a control. All transformants were cultured in an MPY medium.

Analysis of Metabolites of Transformants. BFTPS transformant AO-*fomdF* was seeded in 100 mL of MPY, then scaled to 20 × 3 L Erlenmeyer flasks (1 L of MPY each), and fermented at 30 °C for 3 days. Broth from each flask was centrifuged to collect 1.0 kg of cell biomass. The pellet was acetone-extracted (3 × 1 L), concentrated *in vacuo*, and partitioned with ethyl acetate (EtOAc) (3 × 500 mL). The combined organic layers (2.0 g) were analyzed by GC-MS²² and fractionated by silica gel with petroleum ether (PE) to afford G1–G8. G1 (18.0 mg) was purified by semipreparative RP-HPLC (ACE 5 C18-PFP, 100% MeOH) to give compound 1 (2.0 mg).

FBMN-Guided Discovery of New Mangicols through Heterologous Expression. Compounds that arise from a common

biosynthetic origin often exhibit structural similarities and similar fragmentation patterns. FBMN enables intuitive visualization of potential biosynthetic intermediates and provides evidence for proposing plausible biosynthetic pathways of mangicols. FBMN integrates LC-MS/MS data with molecular networking to map and annotate metabolites by first detecting chromatographic “features” (unique *m/z*–retention time pairs) from raw data using tools like MZmine. These features, representing individual metabolites, are then uploaded to the Global Natural Products Social Molecular Networking (GNPS) platform, where MS/MS spectral similarity groups them into molecular families. In the resulting network, each node represents a metabolite, while edges denote structural relatedness. Annotation is achieved either by direct spectral matching to GNPS databases or by deducing unknown structures based on shared fragmentation patterns and conserved scaffolds within clusters.

To determine products associated with the gene cluster, the transformant AO-*fomd* was cultured in rice medium (640 g) at 30 °C for 5 days. The fermentation material was treated with EtOAc, and the solvent was removed under vacuum to yield a crude extract. Sample analysis used a Shimadzu LC-20AD UPLC instrument connected to a Thermo Scientific Q Exactive Orbitrap mass spectrometer equipped with a positive polarity ESI source. Chromatographic analysis was carried out on a Waters ACQUITY BEH C18 column (150 mm × 4.6 mm, 1.7 μm) using an acidic water/acetonitrile (ACN) gradient as the mobile phase. AO-*fomd* and AO-control extracts (50 μg/mL in MeOH) were analyzed by using an optimized data-dependent acquisition method. The MS workflow consisted of a full scan (*m/z* 100–1200) at a resolution of 70,000 with a scan duration of 50 ms, followed by MS/MS acquisition of the top 10 intense precursor ions via higher-energy collisional dissociation (HCD) at 50 eV, with a resolution of 17,500.

Raw data files were converted to mzXML format using MSconvert,²⁶ and ion peaks were processed in MZmine 2.53, retaining features with MS¹ responsivity exceeding 3.0 × 10⁶ and MS² responsivity above 3.0 × 10³.²¹ The processed data were uploaded to the GNPS platform (<http://gnps.ucsd.edu>) for molecular networking analysis. FBMN was constructed using a minimum cosine score threshold of 0.5 and at least four matched fragment ions, and the resulting network was visualized in Cytoscape v3.7.2. The *m/z* range of 300–600 was selected based on the calculated molecular weight of intermediate compound 1, considering the possible incorporation of one to five oxygen atoms by postmodification enzymes. Raw data files are available at the GNPS under the following task ID: <https://gnps.ucsd.edu/ProteoSAFe/status.jsp?task=39023c07805c4e54b5e0589a19c4b6b2>.

For the isolation and identification of tailored metabolites, AO-*fomd* was cultured under static conditions in 24 kg of rice medium at 30 °C for 18 days with each flask containing 80 g of rice, 120 mL of tap water, and 0.01% adenine. After cultivation, the products were extracted with EtOAc, and the solvent was evaporated under reduced pressure to yield a crude extract (160 g). The extract was partitioned with PE to afford a PE layer (96.4 g), which was fractionated by silica gel column chromatography using a gradient of PE-EtOAc (0 → 100%) to give eight fractions (Fr.1–Fr.8). Fractions Fr.5 and Fr.7 were found to contain possible novel derivatives of mangicdiene (1), as indicated by LC-MS analysis based on characteristic UV spectra and accurate mass measurements. Fr.5 (5.2 g) was further separated by Sephadex LH-20 chromatography using MeOH as the eluent to yield four subfractions (Fr.5.1–Fr.5.4). Fr.5.2 (730.2 mg) was subjected to semipreparative RP-HPLC on a Cholesterol column (10 × 250 mm, 5 μm) and eluted with 80% ACN-H₂O to obtain 7 (4.2 mg) and 2 (25.8 mg). Fr.7 (2.8 g) was purified by Sephadex LH-20 (MeOH 100%) to yield three subfractions (Fr.7.1–Fr.7.3). Fr.7.2 (500.0 mg) was subjected to semipreparative RP-HPLC on an ACE C18-PFP (10 × 250 mm, 5 μm) and eluted with 75% ACN-H₂O to yield 10 (3.0 mg) and Fr.7.2.1 (41.0 mg), which contained chiral compounds. Fr.7.2.1 was further separated using a chiral Daicel Chiralpak IA column (4.6 × 250 mm, 5 μm) and eluted with 95% hexane-ethanol to yield 4 (27.1 mg) and 5 (8.5 mg). Fr.7.3 (452.4 mg) was purified by semipreparative RP-HPLC on a Phenomenex (10

× 250 mm, 5 μ m) and eluted with 80% ACN-H₂O to obtain **9** (1.4 mg), **8** (15.0 mg), **11** (0.4 mg), and Fr.7.3.1 (5.3 mg), which contained chiral compounds. Fr.7.3.1 was further separated on a chiral Daicel Chiralpak IA column (10 × 250 mm, 5 μ m) and eluted with 94% hexane-ethanol to yield **3** (1.2 mg) and **6** (1.4 mg).

Mangicol H (2). Colorless oil. $[\alpha]_D^{20} = +62.7$ (c 2.39, MeOH). HR-ESI-MS m/z 355.2991 $[M-H_2O+H]^+$ (calcd for C₂₅H₃₉O, 355.3001), m/z 373.3096 $[M+H]^+$ (calcd for C₂₅H₄₁O₂, 373.3101). NMR data are compiled in Table S5.

Mangicol M (3). Colorless oil. $[\alpha]_D^{20} = +67.1$ (c 0.14, MeOH). HR-ESI-MS m/z 371.2943 $[M-H_2O+H]^+$ (calcd for C₂₅H₃₉O₂, 371.2950), m/z 389.3046 $[M+H]^+$ (calcd for C₂₅H₄₁O₃, 389.3050). NMR data are compiled in Table S6.

Mangicol N (4). Colorless oil. $[\alpha]_D^{20} = +77.2$ (c 2.48, MeOH). HR-ESI-MS m/z 339.3044 $[M-H_2O+H]^+$ (calcd for C₂₅H₃₉, 339.3052), m/z 357.3147 $[M+H]^+$ (calcd for C₂₅H₄₁O, 357.3152). NMR data are compiled in Table S8.

Mangicol O (5). Colorless oil. $[\alpha]_D^{20} = +43.4$ (c 0.74, MeOH). HR-ESI-MS m/z 339.3044 $[M-H_2O+H]^+$ (calcd for C₂₅H₃₉, 339.3052), m/z 357.3149 $[M+H]^+$ (calcd for C₂₅H₄₁O, 357.3152). NMR data are compiled in Table S9.

Mangicol P (6). Colorless oil. $[\alpha]_D^{20} = +56.7$ (c 0.12, MeOH). HR-ESI-MS m/z 371.2942 $[M-H_2O+H]^+$ (calcd for C₂₅H₃₉O₂, 371.2950), m/z 389.3037 $[M+H]^+$ (calcd for C₂₅H₄₁O₃, 389.3050). NMR data are compiled in Table S10.

Mangicol Q (7). Colorless oil. $[\alpha]_D^{20} = +5.3$ (c 0.30, MeOH). HR-ESI-MS m/z 369.2785 $[M-H_2O+H]^+$ (calcd for C₂₅H₃₇O₂, 369.2794), m/z 387.2888 $[M+H]^+$ (calcd for C₂₅H₃₉O₃, 387.2894). NMR data are compiled in Table S11.

Mangicol R (8). Colorless oil. $[\alpha]_D^{20} = +58.0$ (c 1.40, MeOH). HR-ESI-MS m/z 371.2939 $[M-H_2O+H]^+$ (calcd for C₂₅H₃₉O₂, 371.2950), m/z 389.3044 $[M+H]^+$ (calcd for C₂₅H₄₁O₃, 389.3050). NMR data are compiled in Table S12.

Mangicol D (9). Colorless oil. $[\alpha]_D^{20} = +92.1$ (c 0.14, MeOH). HR-ESI-MS m/z 389.3047 $[M-H_2O+H]^+$ (calcd for C₂₅H₄₁O₃, 389.3050), m/z 407.3155 $[M+H]^+$ (calcd for C₂₅H₄₃O₄, 407.3156). NMR data are compiled in Table S13.

Mangicol S (10). Colorless oil. $[\alpha]_D^{20} = +54.8$ (c 0.31, MeOH). HR-ESI-MS m/z 431.3149 $[M-H_2O+H]^+$ (calcd for C₂₇H₄₃O₄, 431.3161), m/z 449.3253 $[M+H]^+$ (calcd for C₂₇H₄₅O₅, 449.3262). NMR data are compiled in Table S14.

Mangicol T (11). Colorless oil. $[\alpha]_D^{20} = +55.0$ (c 0.06, MeOH). HR-ESI-MS m/z 507.3467 $[M-H_2O+H]^+$ (calcd for C₃₃H₄₇O₄, 507.3474), m/z 525.3571 $[M+H]^+$ (calcd for C₃₃H₄₉O₅, 525.3575). NMR data are compiled in Table S15.

X-ray Single-Crystal Diffraction Experiments. Compound **3** (1.2 mg) was recrystallized in hexane/acetone (2:1, v/v), and the crystallographic data set was collected with a Bruker APEX-II CCD at 180 K using Cu K α radiation. The molecular structure was determined and further refined using the SHELXTL software package. X-ray crystallographic data are presented in Table S7.

Computational Analyses. Conformational exploration was performed by conducting a random search using the MMFF94 force field within Sybyl-X 2.0 software. The obtained geometries were further reoptimized at the B3LYP/6-31G(d) level using Gaussian 09 to yield energy-minimized conformers. ECD spectra of the stable conformers were calculated using time-dependent density functional theory (TDDFT) at the B3LYP/6-31G(d,p) level.²⁷ In addition, theoretical optical rotation values were computed at both the B3LYP/6-31+G(d) and B3LYP/6-311++G(2d,2p) levels.²⁸

Absolute Configurations of the vic-Diols in 6 and 8. Modified Sneath's method was employed as described.^{29,30} Mixtures of compounds **6** and **8** with Mo₂(OAc)₄ in a 1:1.2 molar ratio (1.0 mg/mL in DMSO) were immediately analyzed by ECD. Spectra were monitored over time until a stable profile was achieved (~10 min), after which the intrinsic ECD signals were subtracted. The resulting

induced ECD spectra exhibited diagnostic bands at 310 and 400 nm, whose signs correlated with the *vic*-diols' absolute configuration.

Antimicrobial Assays of the Mangicols. The antimicrobial activities against human pathogenic bacteria (*Staphylococcus aureus* (S. aureus) ATCC6538, methicillin-resistant *S. aureus* JE2, *Staphylococcus epidermidis* (S. epidermidis) CGMCC1.16091, and *Streptococcus mutans* (S. mutans) ATCCUA159) and the human pathogenic fungus (*Candida albicans* (C. albicans) SC5314) were conducted using the nutrient broth dilution method following previously reported protocols.³¹ The nutrient broth dilution method was also used for antifungal activity against five phytopathogenic microbes, including *Ralstonia solanacearum* (R. solanacearum), *Sclerotinia sclerotiorum* (S. sclerotiorum), *Fusarium graminearum* (F. graminearum), *F. oxysporum*, and *Alternaria panax* (A. panax).³² Notably, the assay against *C. albicans* was performed using yeast cells, while the tests for plant pathogens were conducted using spore-based assays.

Antineuroinflammatory Activity In Vitro. Antineuroinflammatory activity was evaluated using mouse microglial BV2 cells. After treatment with the test compounds, an inflammatory response was induced by stimulation with lipopolysaccharide (LPS, 1 μ g/mL). The nitrite concentration released was detected by a Griess reagent system. Detailed experimental procedures were performed according to previously reported methods.³³

Statistical Assay. All experimental data are expressed as the mean \pm standard deviation (SD). Statistical analyses were performed using GraphPad Prism 8.0. The *t* test (and nonparametric tests) was applied to assess the statistical significance of the observed differences.

RESULTS AND DISCUSSION

Bioinformatics Study. Mangicols, initially identified from *F. heterosporum* in 2000,³⁴ represent a class of biologically active sesterterpenoids, with mangicol A and B demonstrating notable anti-inflammatory properties. The precursor mangicdiene is catalyzed by FgMS, a BFTPS derived from *F. graminearum* J1-012.²⁰ Subsequently, a series of novel derivative mangicols H–L were uncovered (Figure S1), among which mangicol J exhibited potent anti-inflammatory activity with low toxicity.¹⁴ The total synthesis of mangicols has proven extremely challenging due to the complexity of their spirotricyclic skeleton, particularly the stereoselective construction of quaternary carbon centers.^{35–37} Given the need for exploring newly biosynthesized analogues, we used BLASTp with FgMS as a query against a database of *F. oxysporum* protein sequences and identified a BFTPS with 76.3% identity and 84.7% similarity to FgMS (Figure S2). The BFTPS was inferred to encode a protein with 767 amino acids and shared a conserved motif with other reported terpene synthases, including the N-terminal ⁹³DDXXD/E⁹⁷ motifs and the ²¹⁹NSE/DTE²²⁷ triad in the TC domain, as well as the C-terminal ⁵¹⁵DDXXD⁵¹⁹ motifs in the PT domain (Figure S3). We initially examined the catalytic function of BFTPS using an *A. oryzae* transformant, AO-*fomdF*. A molecular ion peak at m/z 340 was detected by GC-MS in the ethyl acetate extracts derived from *A. oryzae* transformant cells. Using chromatographic and spectroscopic methods, the major product **1** was obtained and characterized as mangicdiene (Figures S4 and S6–S8),^{20,38} and the BFTPS responsible for its biosynthesis was named FoMS (*Fusarium oxysporum* mangicdiene synthase).

FBMN-Based Discovery of New Mangicols. To explore potential products of mangicols, we carefully examined the flanking regions of *fomdF* and found an uncharacterized six-gene cluster, containing aldo-keto reductase (*fomdB*), monooxygenase (*fomdC*), hydrolase (*fomdG*), and three P450s (*fomdA*, *fomdD*, and *fomdE*) (Figure 1A). Compared

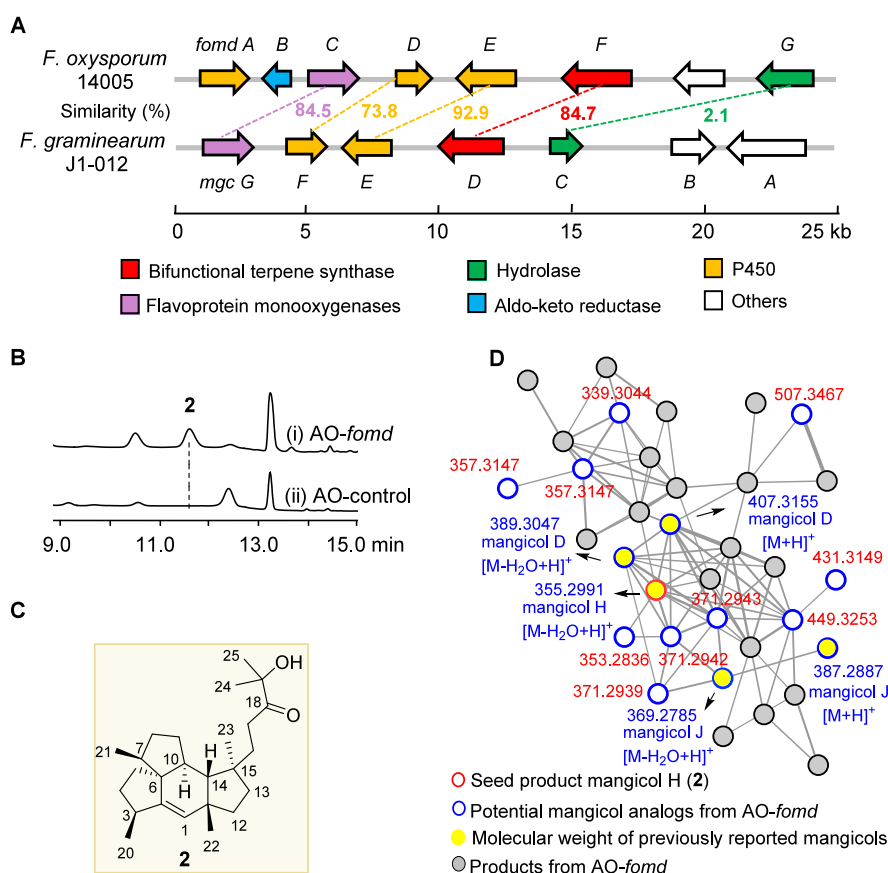


Figure 1. Gene organization and heterologous expression of the *fomd* gene cluster and FBMN-assisted characterization of mangicols D and M–T (3–11). (A) Similarity of the functional genes with homologues in the *mgc* cluster. (B) HPLC profiles of metabolites from transformants AO-*fomd* (i) and AO-control (ii). (C) Structure of mangicol H (2). (D) Molecular networking generated from LC-MS/MS data sets of AO-*fomd* but not found in AO-*fomdF*.

to the *mgc* gene cluster,¹⁴ the *fomd* gene cluster contained a more diverse array of modification enzymes, including an additional P450 enzyme (FomdA) and an aldo-keto reductase (FomdB), which may facilitate the introduction of diverse functional groups into the mangicol skeleton. FomdA exhibited 65.7% sequence similarity to EqxH, a putative oxidase involved in equisetin biosynthesis,³⁹ while FomdB exhibited 48.1% sequence similarity to an aldehyde-reducing enzyme reported to catalyze the selective conversion of aflatoxin B1 dialdehyde.⁴⁰ The five remaining proteins (FomdC–FomdG) all have homologous counterparts in the *mgc* gene cluster. Except for the hydrolase (FomdG), which has no significant similarity to its homologue MgcC with a low similarity of 2.1%, the other four proteins (FomdC–FomdF) share high similarity with their respective homologues at 84.5, 73.8, 92.9, and 84.7% (Figure 1A and Table S1).

The transformant AO-*fomd* harboring all these genes (*fomdA*–*fomdG*), was constructed to expand the chemical space of mangicol-type sesterterpenoids. Small-scale (640 g of rice) fermentation of the gene cluster transformant AO-*fomd* was performed, and the extract was analyzed and monitored by LC-MS. Compound 2 was the major product compared to the control (Figure 1B). Comparison of the NMR data and optical rotation of compound 2 with previously reported values (Table S5 and Figures S9–S15) identified it as the known compound mangicol H (Figure 1C).¹⁴

To uncover associated products, compound 2 was used as a seed via FBMN for the recognition of AO-*fomd* transformant-

associated nodes from LC-MS/MS data sets. We found that 34 nodes from AO-*fomd* were associated with compound 2. After detailed analysis of their HRMS data, 14 nodes predicted as sesterterpenoids were screened out and marked as blue circles in the network (Figure 1D, Figure S5, and Table S4). Some of these nodes showed the same molecular weight as previously reported compounds, such as mangicol D (m/z 407.3155 $[M + H]^+$)³⁴ and mangicol J (m/z 387.2888 $[M + H]^+$),¹⁴ while the majority of the other nodes corresponded to entirely new molecular weights. This suggested that the *fomd* gene cluster may catalyze a series of mangicol-related analogs with different carbon backbones.

Structural Characterization of Mangicols (3–11).

Isolation and characterization of these selected nodes from large-scale fermentation of AO-*fomd* (25 kg rice medium) led to the characterization of eight new derivatives (3–8, 10, and 11) and one previously reported compound mangicol D (9) (Figure 2A). NMR spectral analysis indicated that all newly identified compounds retained the ring system as mangicdiene (1) (Figure 2B).

Compound 3 exhibited ¹H and ¹³C NMR spectra closely resembling those of compound 2 (Table S6 and Figures S16–S22). The obvious difference was the presence of a pentacyclic group and the absence of a keto group in 3, as supported by the HMBC correlations from H₃-25 to C-18, C-19, and C-24 and from H₂-24 to C-17, C-18, C-19, and C-25 (Figure S81A). The relative configuration of 3 was assigned based on NOESY correlations observed between H-23/H-10/H-16b/H-17, H-

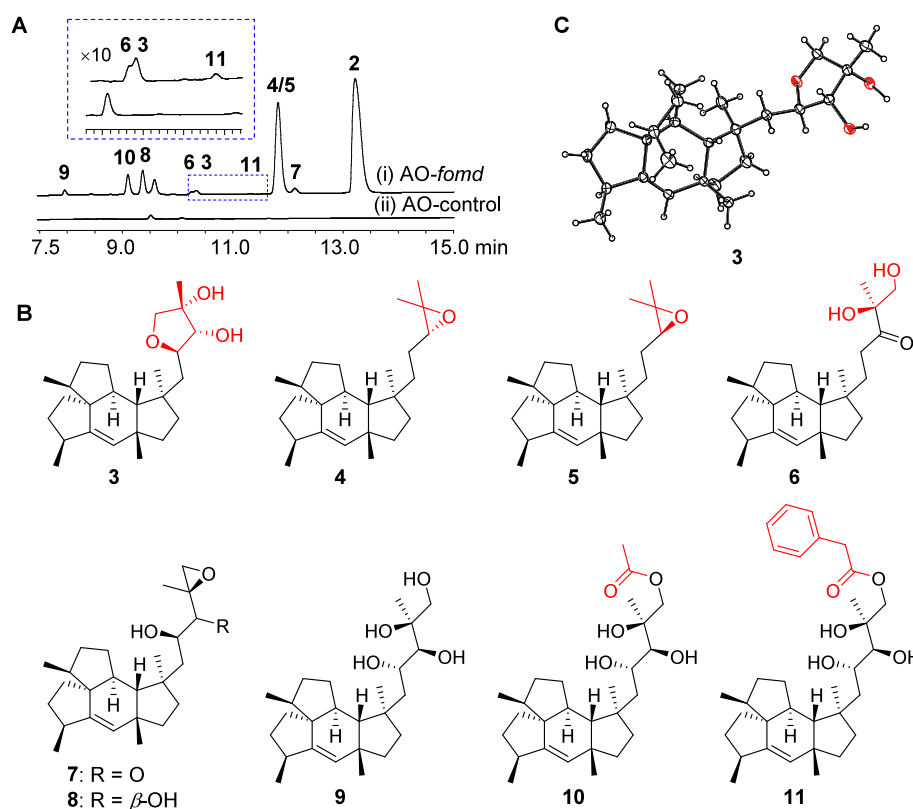


Figure 2. Structures of mangicols identified from AO-fomd. (A) LC-MS profiles of metabolites from AO-fomd (i) and AO-control (ii). (B) Structures of mangicols D and M-T (3–11). The groups marked in red in the side chains are newly discovered in this study. (C) X-ray crystallographic structure of 3.

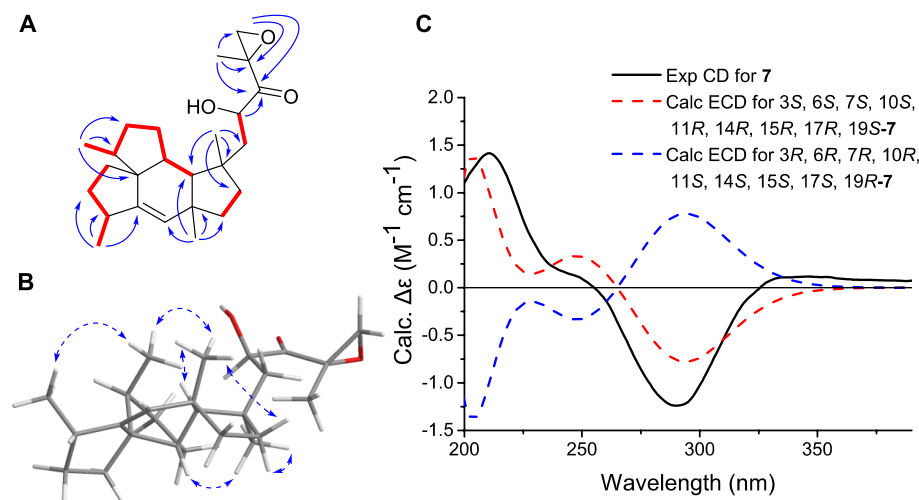


Figure 3. Key 2D NMR correlations and ECD spectrum of compound 7. (A) Key ¹H–¹H COSY (bold) and HMBC (arrow) correlations of 7. (B) Key NOESY correlations of 7. (C) Calculated and experimental ECD spectra of 7.

17/H-13a, H-22/H-12b/H-13b/H-14/H-21, and H-20/H-21 (Figure S81B). The above findings were additionally validated by an X-ray single-crystal diffraction experiment (Figure 2C and Table S7, CCDC 2099502). Thereby, the structure of 3 was assigned to 3S, 6S, 7S, 10S, 11R, 14R, 15R, 17R, 18R, and 19S.

Compounds 4 and 5, a pair of epimers, were obtained by chiral separation using HPLC with a Chiralpak IA column. The ¹H and ¹³C NMR data of 4 and 5 (Tables S8 and S9 and Figures S23–S36) exhibited strong similarity to those of 1,

except for the introduction of an epoxy group between C-18 and C-19, in place of the double bond present in 1 (Figure S81A). The absolute stereochemistry of 4 and 5 was established as 18R and 18S, respectively, based on the comparison of experimental optical rotation with calculated data (Tables S16–S19 and Figures S82 and S83).

The ¹H and ¹³C NMR data of compound 6 (Table S10 and Figures S37–S43) closely resembled those of compound 2. A notable distinction was the presence of an extra hydroxyl group located at C-24 (δ_c 69.8) in 6, as indicated by HMBC

Table 1. Antimicrobial Activity against Plant and Human Pathogens

compound	pathogens (MIC, μM)				
	<i>R. solanacearum</i>	<i>S. aureus</i> JE2	<i>S. epidermidis</i>	<i>S. aureus</i> 6538	<i>S. mutans</i>
3	>50	25	25	12.5	12.5
6	>50	>50	>50	12.5	6.25
7	>50	>50	>50	25	25
8	6.25	25	25	25	12.5
9	12.5	>50	>50	>50	>50
ciprofloxacin ^a	3.13	NT	NT	NT	NT
vancomycin ^a	NT	1	NT	NT	NT
oxacillin ^a	NT	NT	2	2	NT
chlorhexidine ^a	NT	NT	NT	NT	2

^aPositive control. NT, Not tested.

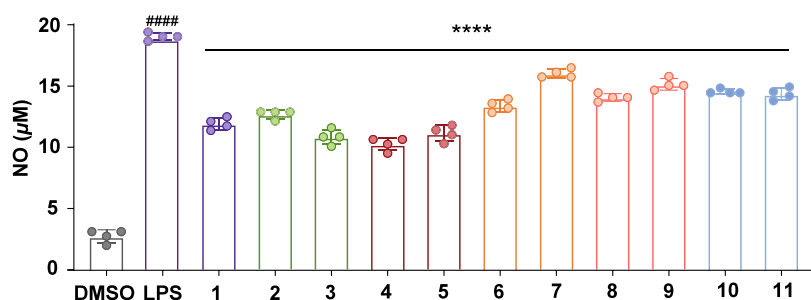


Figure 4. Inhibitory effects of compounds 1–11 against LPS-induced NO production in BV2 cells. The mean \pm SD of four replicates is shown. **** p < 0.001 with the LPS group, ### p < 0.001 with the control group.

correlations from H₂-17 to C-15 and C-18, from H₃-25 to C-18, C-19, and C-24, and from H₂-24 to C-18, C-19, and C-25 in **6** (Figure S81A). Due to the presence of the 19,24-diol moiety in **6**, the absolute configuration of C-19 was determined by the induced ECD spectrum of its in situ complex with Mo₂(OAc)₄ in DMSO solution.³⁰ The ECD spectrum exhibited a positive Cotton effect at 293.5 nm (Figure S84),⁴¹ which permitted the assignment of the 19S absolute configuration of **6**.

Compound **7** has the same relative configuration with the known product mangicol J (Table S11 and Figures S44–S50).¹⁴ The absolute configurations at C-17 and C-19 were further assigned as 17R and 19S based on computational ECD analysis (Figure 3, Figure S85, and Table S20).

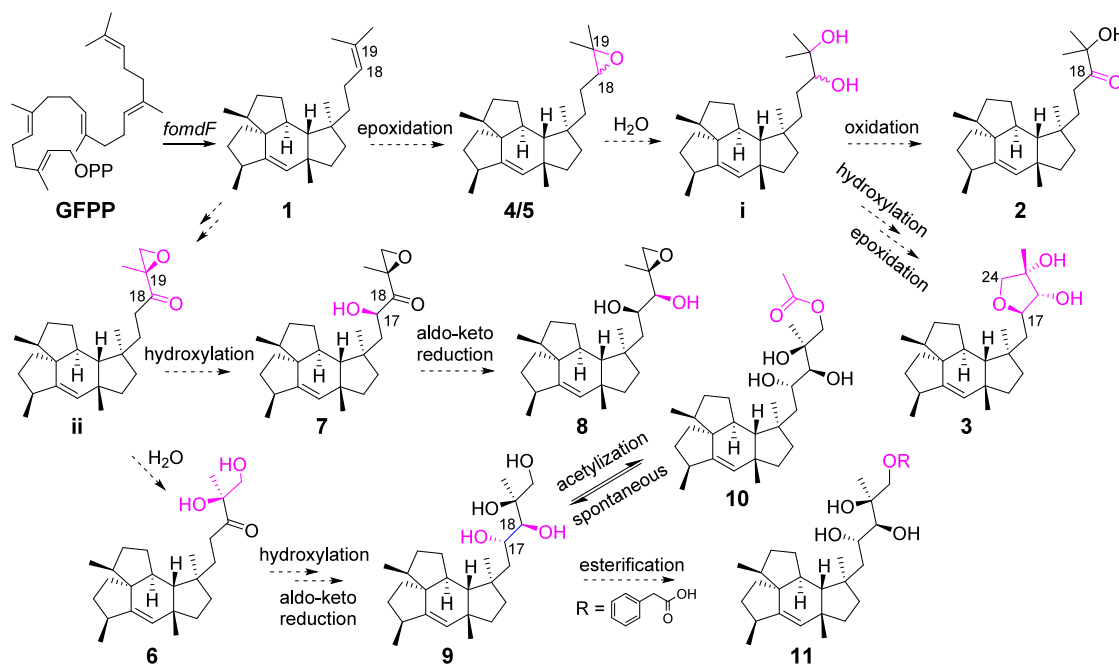
Compound **8** showed the same planar structure as the known product, mangicol G (Table S12 and Figures S51–S57),³⁴ whose absolute configuration has not been reported previously. The NOESY correlations of H-17/H-18/H-23 with the coupling constant ($J_{\text{H-17/H-18}} = 4.2$ Hz) indicated the erythron orientation of H-17 and H-18 in **8**. The absolute configuration of the 17,18-diol system in **8** was also defined by the modified Snetzke's method. Upon complexation with Mo₂(AcO)₄ in DMSO, the induced CD spectrum exhibited a negative Cotton effect at 310 nm (Figure S86), indicative of negative helicity of the O–C–C–O segment, thereby supporting the assignment of the 17R and 18S configurations for **8**.

Through comparison of the NMR and optical rotation data with those reported in the literature, compound **9** was identified as the previously characterized product, mangicol D (Table S13 and Figures S58–S66).³⁴ The ¹H and ¹³C NMR data of **10** and **11** (Tables S14 and S15 and Figures S67–S80) closely matched those of **9**. In **10**, a notable difference was the presence of an extra acetyl moiety at C-24 (δ_{C} 71.2), as

supported by the HMBC correlation from H₂-24 to the carbonyl carbon (δ_{C} 171.4) of the acetyl group (Figure S81A). We found that compound **10** could spontaneously transform into compound **9** at room temperature. In **11**, a phenylacetyl group at C-24 (δ_{C} 71.5) replaced a hydrogen as found in **9**, as evidenced by the HMBC interactions from H₂-24 to C-26 and from H₂-27 to C-26, C-28, C-29, and C-33 (Figure S81A). In addition to the terminal epoxide formation reported uniformly in the literature between C-19 and C-24, this study also identified two additional instances of terminal epoxide formations between C-17 and C-24 and between C-18 and C-19. In contrast to the *mgc* gene cluster, which catalyzed only the formation of a carbonyl group at C-18 in the side chain, the *fomd* gene cluster can catalyze the simultaneous formation of a carbonyl group and a hydroxyl group at C-18. Notably, mangicol P as the terminal epoxy ring-opening product of mangicol I was obtained, and this has not been reported for products catalyzed by *mgc*. Furthermore, starting with compound **9**, more complex compounds **10** and **11** were derived, which indicated that more analogs may be obtained by further derivatization based on existing side chains. The above results confirmed that the *fomd* gene cluster can greatly enrich the diversity of mangicol side chain groups.

Biological Activity. Compounds 1–11 were evaluated for antimicrobial efficacy against both phytopathogenic microorganisms and common foodborne human pathogens. The plant pathogen *R. solanacearum*, which causes lethal wilt disease, is a bacterial species known to infect more than 200 plant hosts spanning upward of 50 different plant families.^{42,43} Among the tested compounds, **8** and **9** showed good activity against *R. solanacearum*, with MIC values of 6.25 and 12.5 μM , respectively. The antibiotic resistance of Gram-positive cocci, particularly *S. aureus* and *Streptococcus* species, poses a major public health threat, with *S. aureus* being a frequent cause of

Scheme 1. Hypothetical Biosynthetic Pathway of 1–11



foodborne illnesses.^{44,45} Antibacterial assays revealed that compounds 3 and 8 demonstrated activity against *S. aureus* JE2, *S. epidermidis*, and *S. aureus* 6538, with MIC values ranging from 12.5 to 25 μ M. Additionally, compounds 6 and 7 displayed inhibitory activity against *S. aureus* 6538, showing MIC values of 12.5 and 25 μ M, respectively. Compounds 3 and 6–8 also exhibited antibacterial activity against the oral pathogen *S. mutans*, with MIC values ranging from 6.25 to 25 μ M (Table 1). These results suggested that a vicinal diol in the side chain may play a key role in inhibiting *S. aureus*, while the epoxy and carbonyl groups may further modulate this antimicrobial activity. All tested compounds were inactive against both plant and human fungal pathogens (Tables S21 and S22).

In addition to antimicrobial assays, the antineuroinflammatory potential of isolated compounds was assessed by evaluating their effects on LPS-induced nitric oxide (NO) production in BV2 microglial cells. Compounds 3–5 all at 10 μ M showed appreciable anti-inflammatory effects, with NO inhibition rates of 50.0, 53.13, and 48.05%, respectively. In contrast, the remaining compounds showed relatively weak anti-inflammatory effects (Figure 4 and Table S23).

Compared with previously reported mangicols, newly identified compounds 1–11 exhibit both overlapping and distinct bioactivities. Mangicols A, B, and J were primarily reported for their anti-inflammatory properties, with mangicol A showing potent inhibition of phorbol myristate acetate (PMA)-induced ear edema in mice (81% reduction)³⁴ and mangicol J demonstrating potent NO inhibition in RAW264.7 cells (IC_{50} = 8.29 μ M) without cytotoxicity.¹⁴ In our study, compounds 3–5 exhibited comparable anti-inflammatory activity in BV2 microglial cells, with NO inhibition rates around 50% at 10 μ M. Notably, antimicrobial activity has not been reported for known mangicols, whereas several of our compounds, particularly 3 and 6–9, demonstrated notable inhibitory activity toward *S. aureus*, *S. mutans*, and *R. solanacearum*, with MIC values as low as 6.25 μ M. These findings suggest that the new analogues expand the biological

scope of the mangicol scaffold, exhibiting both anti-inflammatory and previously unrecognized antibacterial activities.

Proposed Biosynthetic Pathway of New Mangicols.

Based on their chemical structures, we propose this possible biosynthetic pathway for compounds 1–11 (Scheme 1). The pathway starts with the GFPP catalyzed by *fmdF* to generate 1, followed by the stereoselective epoxidation of the terminal olefin to yield 4 and 5,^{14,46} which undergo ring-opening hydrolysis to form presumed product i and then further oxidation of the C18-hydroxyl to yield 2.⁴⁶ The i could be hydroxylated as well at C-17 and C-24, with further etherification to generate 3. The proposed reaction pathway entails a P450-mediated hydroxylation at C-17 under aerobic conditions, which facilitates an intramolecular nucleophilic attack at C-24, ultimately leading to the construction of the furan ring.^{47,48} Simultaneously, there was another terminal epoxidation at 1 to form presumed product ii and then hydroxylation at C-17 to yield 7, which further undergoes keto reduction at C-18 to afford 8.⁴⁹ The ring-opening hydrolysis of the terminal epoxy of ii provides 6, which further undergoes hydroxylation at C-17 and keto reduction at C-18 to obtain 9, which may be acetylated by endogenous acetyl transferase of *A. oryzae* to generate 10.^{50,51} The condensation between 9 and a phenylalanine derivative (phenylacetic acid) produces 11.^{14,52,53} Notably, 10 could be converted into 9 spontaneously without the involvement of hydrolase, which is different from the hydrolysis of the 17-O-acetyl side chain of demethoxyviridin, which requires the participation of esterase.⁵⁴

In conclusion, the biosynthetic pathway for mangicols from *F. oxysporum* was successfully elucidated through bioinformatics and experimental approaches. A new BFTPS, FoMS, was identified, showing a high sequence similarity to FgMS from *F. graminearum* and catalyzing the production of mangicdiene. Further investigation of the flanking gene cluster revealed several novel enzymes involved in the modification of the mangicols. Integration of heterologous expression with

FBMN strategies has facilitated the generation and identification of eight novel derivatives of mangicol. Biological assays demonstrated significant antimicrobial and antineuroinflammatory activities for several of these new derivatives, particularly against *R. solanacearum*, *S. mutans*, and some other foodborne pathogens. The proposed biosynthetic pathway provides insight into the enzymatic steps involved, paving the way for further optimization to enhance the production of these promising compounds. These findings expand the diversity of mangicol-type sesterterpenoids and highlight their potential as bioactive compounds with therapeutic applications, not only aiding contamination prevention but also enhancing the nutritional functionality of food products.

■ ASSOCIATED CONTENT

SI Supporting Information

The Supporting Information is available free of charge at <https://pubs.acs.org/doi/10.1021/acs.jafc.5c04187>.

Molecular network grouping MS/MS data, HR-EI-MS spectrum of **1**; HR-ESI-MS spectra of **2–11**; 1D NMR spectrum of **1**; 1D and 2D NMR spectra of **2–11**; X-ray crystallographic data for compound **3**, ECD calculation details, and antifungal activities of compounds against human and plant pathogenic microbes (PDF)

■ AUTHOR INFORMATION

Corresponding Authors

Lan Jiang – Department of Cardiothoracic Surgery, Children's Hospital of Nanjing Medical University, Nanjing 210093, China; Email: jianglan0426@163.com

Xueteng Liu – State Key Laboratory of Bioreactor Engineering, East China University of Science and Technology, Shanghai 200237, China; orcid.org/0000-0002-1322-8253; Email: liuxueteng@ecust.edu.cn

Authors

Cuiping Xing – State Key Laboratory of Bioreactor Engineering, East China University of Science and Technology, Shanghai 200237, China

Huanting Yang – State Key Laboratory of Bioreactor Engineering, East China University of Science and Technology, Shanghai 200237, China

Kangjie Lv – State Key Laboratory of Bioreactor Engineering, East China University of Science and Technology, Shanghai 200237, China

Keying Lan – State Key Laboratory of Bioreactor Engineering, East China University of Science and Technology, Shanghai 200237, China

Guoliang Zhu – State Key Laboratory of Bioreactor Engineering, East China University of Science and Technology, Shanghai 200237, China; orcid.org/0000-0002-6628-8874

Bin Zhu – State Key Laboratory of Bioreactor Engineering, East China University of Science and Technology, Shanghai 200237, China; orcid.org/0000-0003-1085-1231

Biao Ren – State Key Laboratory of Oral Diseases & National Clinical Research Center for Oral Diseases, West China Hospital of Stomatology, Sichuan University, Chengdu 610041, China; orcid.org/0000-0003-4215-2873

Yi Jiang – The Key Lab for Research & Development of Actinomycete Resources, Yunnan Institute of Microbiology, Yunnan University, Kunming 650500, China

Chenglin Jiang – The Key Lab for Research & Development of Actinomycete Resources, Yunnan Institute of Microbiology, Yunnan University, Kunming 650500, China

Huanqin Dai – Key Laboratory of Pathogenic Microbiology and Immunology, Institute of Microbiology, Chinese Academy of Sciences, Beijing 100101, China

Xuming Mo – Department of Cardiothoracic Surgery, Children's Hospital of Nanjing Medical University, Nanjing 210093, China

Tom Hsiang – School of Environmental Sciences, University of Guelph, Guelph, Ontario N1G2W1, Canada

Wael M. Abdelmageed – Department of Pharmacognosy, Faculty of Pharmacy, Assiut University, Assiut 71526, Egypt; orcid.org/0000-0002-8130-684X

Lixin Zhang – State Key Laboratory of Bioreactor Engineering, East China University of Science and Technology, Shanghai 200237, China

Complete contact information is available at: <https://pubs.acs.org/doi/10.1021/acs.jafc.5c04187>

Notes

The authors declare no competing financial interest.

■ ACKNOWLEDGMENTS

We acknowledge the generous funding received from the Shanghai Sci-Tech Inno Center for Infection & Immunity (SSIII-2024A01 and SSIII-2024A02), Shanghai Municipal Science and Technology Major Project, National Key Research and Development Program of China (2020YFA090032 and 2019YFA0906200), National Natural Science Foundation of China (21977029 and 81903529), Open Project Funding of the State Key Laboratory of Bioreactor Engineering, and 111 Project (B18022). We are grateful to Prof. Hideaki Oikawa (Hokkaido University) for his kind guidance. The genome of strain FO14005 was sequenced and assembled with financial support from the Natural Sciences and Engineering Research Council of Canada, awarded to Prof. T. Hsiang.

■ REFERENCES

- (1) Murray, C. J. L.; Ikuta, K. S.; Sharara, F.; Swetschinski, L.; Robles Aguilar, G.; Gray, A.; Han, C.; Bisignano, C.; Rao, P.; Wool, E.; et al. Global burden of bacterial antimicrobial resistance in 2019: a systematic analysis. *Lancet* **2022**, 399 (10325), 629–655.
- (2) Annunziato, G. Strategies to overcome antimicrobial resistance (AMR) making use of non-essential target inhibitors: A Review. *Int. J. Mol. Sci.* **2019**, 20 (23), 5844.
- (3) Fisher, M. C.; Hawkins, N. J.; Sanglard, D.; Gurr, S. J. Worldwide emergence of resistance to antifungal drugs challenges human health and food security. *Science* **2018**, 360 (6390), 739–742.
- (4) Mousavi Khaneghah, A.; Abhari, K.; Eg, I.; Soares, M. B.; Oliveira, R. B. A.; Hosseini, H.; Rezaei, M.; Balthazar, C. F.; Silva, R.; Cruz, A. G.; Ranadheera, C. S.; Sant'Ana, A. S. Interactions between probiotics and pathogenic microorganisms in hosts and foods: A review. *Trends Food Sci. Technol.* **2020**, 95, 205–218.
- (5) Doeblemann, G.; Ökmen, B.; Zhu, W.; Sharon, A.; Heitman, J.; Howlett, B. J. Plant pathogenic fungi. *Microbiol. Spectr.* **2017**, 5, 1–23.
- (6) Fang, G. Y.; Wu, F. H.; Mu, X. J.; Jiang, Y. J.; Liu, X. Q. Monitoring longitudinal antimicrobial resistance trends of *Staphylococcus aureus* strains worldwide over the past 100 years to decipher its evolution and transmission. *J. Hazard. Mater.* **2024**, 465, No. 133136.

- (7) Speziale, P.; Rindi, S.; Pietrocola, G. Antibody-based agents in the management of antibiotic-resistant *Staphylococcus aureus* diseases. *Microorganisms* **2018**, *6* (1), 25.
- (8) Mansfield, J.; Genin, S.; Magori, S.; Citovsky, V.; Sriariyanum, M.; Ronald, P.; Dow, M.; Verdier, V.; Beer, S. V.; Machado, M. A.; Toth, I.; Salmond, G.; Foster, G. D. Top 10 plant pathogenic bacteria in molecular plant pathology. *Mol. Plant Pathol.* **2012**, *13* (6), 614–629.
- (9) Salanoubat, M.; Genin, S.; Artiguenave, F.; Gouzy, J.; Mangenot, S.; Arlat, M.; Billault, A.; Brottier, P.; Camus, J. C.; Cattolico, L.; Chandler, M.; Choisine, N.; Claudel-Renard, C.; Cunnac, S.; Demange, N.; Gaspin, C.; Lavie, M.; Moisan, A.; Robert, C.; Saurin, W.; Schiex, T.; Siguier, P.; Thébault, P.; Whalen, M.; Wincker, P.; Levy, M.; Weissenbach, J.; Boucher, C. A. Genome sequence of the plant pathogen *Ralstonia solanacearum*. *Nature* **2002**, *415* (6871), 497–502.
- (10) Luo, P.; Huang, J. H.; Lv, J. M.; Wang, G. Q.; Hu, D.; Gao, H. Biosynthesis of fungal terpenoids. *Nat. Prod. Rep.* **2024**, *41* (5), 748–783.
- (11) Yin, Z.; Dickschat, J. S. J. N. P. R. Engineering fungal terpene biosynthesis. *Nat. Prod. Rep.* **2023**, *40* (1), 28–45.
- (12) Chen, S.; Cai, R.; Liu, Z.; Cui, H.; She, Z. Secondary metabolites from mangrove-associated fungi: source, chemistry and bioactivities. *Nat. Prod. Rep.* **2022**, *39* (3), 560–595.
- (13) Shi, Y.; Ji, M.; Dong, J.; Shi, D.; Wang, Y.; Liu, L.; Feng, S.; Liu, L. New bioactive secondary metabolites from fungi: 2023. *Mycology* **2024**, *15* (3), 283–321.
- (14) Yuan, Y.; Cheng, S.; Bian, G.; Yan, P.; Ma, Z.; Dai, W.; Chen, R.; Fu, S.; Huang, H.; Chi, H.; Cai, Y.; Deng, Z.; Liu, T. Efficient exploration of terpenoid biosynthetic gene clusters in filamentous fungi. *Nat. Catal.* **2022**, *5* (4), 277–287.
- (15) Evidente, A. The incredible story of ophiobolin A and sphaeropsidin A: two fungal terpenes from wilt-inducing phytotoxins to promising anticancer compounds. *Nat. Prod. Rep.* **2024**, *41* (3), 434–468.
- (16) Verbist, L. The antimicrobial activity of fusidic acid. *J. Antimicrob. Chemother.* **1990**, *25* (suppl. B), 1–5.
- (17) Christianson, D. W. Structural and chemical biology of terpenoid cyclases. *Chem. Rev.* **2017**, *117* (17), 11570–11648.
- (18) Toyomasu, T.; Tsukahara, M.; Kaneko, A.; Niida, R.; Mitsushashi, W.; Dai, T.; Kato, N.; Sassa, T. Fusicoccins are biosynthesized by an unusual chimera diterpene synthase in fungi. *Proc. Natl. Acad. Sci. U.S.A.* **2007**, *104* (9), 3084–3088.
- (19) Li, K.; Gustafson, K. R. Sesterterpenoids: chemistry, biology, and biosynthesis. *Nat. Prod. Rep.* **2021**, *38* (7), 1251–1281.
- (20) Bian, G.; Han, Y.; Hou, A.; Yuan, Y.; Liu, X.; Deng, Z.; Liu, T. Releasing the potential power of terpene synthases by a robust precursor supply platform. *Metab. Eng.* **2017**, *42*, 1–8.
- (21) Nothias, L. F.; Petras, D.; Schmid, R.; Dührkop, K.; Rainer, J.; Sarvepalli, A.; Protsyuk, I.; Ernst, M.; Tsugawa, H.; Fleischauer, M.; et al. Feature-based molecular networking in the GNPS analysis environment. *Nat. Methods* **2020**, *17* (9), 905–908.
- (22) Jiang, L.; Zhang, X.; Sato, Y.; Zhu, G.; Minami, A.; Zhang, W.; Ozaki, T.; Zhu, B.; Wang, Z.; Wang, X.; Lv, K.; Zhang, J.; Wang, Y.; Gao, S.; Liu, C.; Hsiang, T.; Zhang, L.; Oikawa, H.; Liu, X. Genome-based discovery of enantiomeric pentacyclic sesterterpenes catalyzed by fungal bifunctional terpene synthases. *Org. Lett.* **2021**, *23* (12), 4645–4650.
- (23) Jiang, L.; Yang, H.; Zhang, X.; Li, X.; Lv, K.; Zhang, W.; Zhu, G.; Liu, C.; Wang, Y.; Hsiang, T.; Zhang, L.; Liu, X. Schultriene and nigtetraene: two sesterterpenes characterized from pathogenic fungi via genome mining approach. *Appl. Microbiol. Biotechnol.* **2022**, *106* (18), 6047–6057.
- (24) Jin, F. J.; Maruyama, J. i.; Juvvadi, P. R.; Arioka, M.; Kitamoto, K. Development of a novel quadruple auxotrophic host transformation system by *argB* gene disruption using *adeA* gene and exploiting adenine auxotrophy in *Aspergillus oryzae*. *FEMS Microbiol. Lett.* **2004**, *239* (1), 79–85.
- (25) Oikawa, H. Reconstitution of biosynthetic machinery of fungal natural products in heterologous hosts. *Biosci. Biotechnol. Biochem.* **2020**, *84* (3), 433–444.
- (26) Chambers, M. C.; Maclean, B.; Burke, R.; Amodei, D.; Ruderman, D. L.; Neumann, S.; Gatto, L.; Fischer, B.; Pratt, B.; Egertson, J.; et al. A cross-platform toolkit for mass spectrometry and proteomics. *Nat. Biotechnol.* **2012**, *30* (10), 918–920.
- (27) Lv, K.; Duan, Y.; Li, X.; Wang, X.; Xing, C.; Lan, K.; Zhu, B.; Zhu, G.; Qiu, Y.; Li, S.; Hsiang, T.; Zhang, L.; Jiang, L.; Liu, X. Identifying sesterterpenoids via feature-based molecular networking and small-scale fermentation. *Appl. Microbiol. Biotechnol.* **2024**, *108* (1), 483.
- (28) Stephens, P. J.; Devlin, F. J.; Cheeseman, J. R.; Frisch, M. J. Calculation of optical rotation using density functional theory. *J. Phys. Chem. A* **2001**, *105* (22), 5356–5371.
- (29) Di Bari, L.; Pescitelli, G.; Pratelli, C.; Pini, D.; Salvadori, P. Determination of absolute configuration of acyclic 1,2-Diols with Mo₂(OAc)₄. 1. Snatzke's Method Revisited. *J. Org. Chem.* **2001**, *66* (14), 4819–4825.
- (30) Cai, R.; Jiang, H.; Mo, Y.; Guo, H.; Li, C.; Long, Y.; Zang, Z.; She, Z. Ophiobolin-type sesterterpenoids from the mangrove endophytic fungus *Aspergillus* sp. ZJ-68. *J. Nat. Prod.* **2019**, *82* (8), 2268–2278.
- (31) Li, Y.; Zhu, G.; Wang, J.; Yu, J.; Ye, K.; Xing, C.; Ren, B.; Zhu, B.; Chen, S.; Lai, L.; Li, Y.; Hsiang, T.; Zhang, L.; Liu, X.; Zhang, J. New polyketide congeners with antibacterial activities from an endophytic fungus *Stemphylium globuliferum* 17035 (China General Microbiological Culture Collection Center No. 40666). *J. Fungi* **2024**, *10* (11), 737.
- (32) Wang, D.; Wang, C.; Gui, P.; Liu, H.; Khalaf, S. M. H.; Elsayed, E. A.; Wadaan, M. A. M.; Hozzein, W. N.; Zhu, W. Identification, bioactivity, and productivity of actinomycins from the marine-derived *Streptomyces heliomycini*. *Front. Microbiol.* **2017**, *8*, 1147.
- (33) Zou, Z. B.; Wu, T. Z.; Yang, L. H.; He, X. W.; Liu, W. Y.; Zhang, K.; Xie, C. L.; Xie, M. M.; Zhang, Y.; Yang, X. W.; Wang, J. S. Hepialiamides A–C: aminated fusaric acid derivatives and related metabolites with anti-inflammatory activity from the deep-sea-derived fungus *Samsoniella hepiali* W7. *Mar. Drugs* **2023**, *21* (11), 596.
- (34) Renner, M. K.; Jensen, P. R.; Fenical, W. Mangicols: structures and biosynthesis of a new class of sesterterpene polyols from a marine fungus of the genus *Fusarium*. *J. Org. Chem.* **2000**, *65* (16), 4843–4852.
- (35) Araki, K.; Saito, K.; Arimoto, H.; Uemura, D. J. A. C. I. E. Enantioselective synthesis of the spirotricyclic carbon core of mangicols by using a stereoselective transannular Diels-Alder strategy. *Angew. Chem., Int. Ed.* **2004**, *43* (1), 81–84.
- (36) Pichlmair, S.; de Lera Ruiz, M.; Vilotijevic, I.; Paquette, L. A. Exploration of conjugate addition routes to advanced tricyclic components of mangicol A. *Tetrahedron* **2006**, *62* (24), 5791–5802.
- (37) Pichlmair, S.; de Lera Ruiz, M.; Basu, K.; Paquette, L. A. Evaluation of possible intramolecular [4 + 2] cycloaddition routes for assembling the central tetracyclic core of the potent marine antiinflammatory agent mangicol A. *Tetrahedron* **2006**, *62* (22), 5178–5194.
- (38) Luo, P.; Lv, J. M.; Zhen, H. T.; Zhao, Y. Q.; Liu, J. Y.; Hong, J. Y.; Li, S. Y.; Wang, G. Q.; Chen, G. D.; Zhang, S. X.; Hu, D.; Gao, H. Identification of two novel sesterterpene skeletons offers the first experimental evidence for the cyclization mechanism of mangidiene synthase. *Chin. Chem. Lett.* **2025**, No. 111042.
- (39) Kakule, T. B.; Sardar, D.; Lin, Z.; Schmidt, E. W. Two related pyrrolidinedione synthetase loci in *Fusarium heterosporum* ATCC 74349 produce divergent metabolites. *ACS Chem. Biol.* **2013**, *8* (7), 1549–1557.
- (40) Wu, J.; Xu, W.; Zhang, C.; Chang, Q.; Tang, X.; Li, K.; Deng, Y. Trp266 determines the binding specificity of a porcine aflatoxin B1 aldehyde reductase for aflatoxin B1-dialdehyde. *Biochem. Pharmacol.* **2013**, *86* (9), 1357–1365.
- (41) Hou, Y.; Li, Q.; Chen, M.; Wu, H.; Yang, J.; Sun, Z.; Xu, X.; Ma, G. Novel geranylhydroquinone derived meroterpenoids from the

fungus *Clitocybe clavipes* and their cytotoxic activity. *Fitoterapia* **2022**, 161, No. 105251.

(42) Genin, S. Molecular traits controlling host range and adaptation to plants in *Ralstonia solanacearum*. *New Phytol.* **2010**, 187 (4), 920–928.

(43) Huet, G. Breeding for resistances to *Ralstonia solanacearum*. *Front. Plant Sci.* **2014**, 5, 715.

(44) Carapetis, J. R.; Steer, A. C.; Mulholland, E. K.; Weber, M. The global burden of group A streptococcal diseases. *Lancet Infect Dis* **2005**, 5 (11), 685–694.

(45) Gordon, R. J.; Lowy, F. D. Pathogenesis of methicillin-resistant *Staphylococcus aureus* infection. *Clin. Infect. Dis.* **2008**, 46 (Supplement 5), S350–S359.

(46) Araki, Y.; Awakawa, T.; Matsuzaki, M.; Cho, R.; Matsuda, Y.; Hoshino, S.; Shinohara, Y.; Yamamoto, M.; Kido, Y.; Inaoka, D. K.; Nagamune, K.; Ito, K.; Abe, I.; Kita, K. Complete biosynthetic pathways of ascofuranone and ascochlorin in *Acremonium egyptiacum*. *Proc. Natl. Acad. Sci. U.S.A.* **2019**, 116 (17), 8269–8274.

(47) Kwon, M.; Utomo, J. C.; Park, K.; Pascoe, C. A.; Chiorean, S.; Ngo, I.; Pelot, K. A.; Pan, C. H.; Kim, S. W.; Zerbe, P.; Vederas, J. C.; Ro, D. K. Cytochrome P450-catalyzed biosynthesis of a dihydrofuran neoclerodane in magic mint (*Salvia divinorum*). *ACS Catal.* **2022**, 12 (1), 777–782.

(48) Sun, T.; Liu, M.; Li, S.; Guo, J.; Liu, L.; Zhang, L.; Ma, L.; Li, S. Cytochrome P450-catalyzed tetrahydrofuran formation via dual pathways in avermectin biosynthesis. *ACS Catal.* **2025**, 15 (4), 3295–3305.

(49) Matsuda, Y.; Quan, Z.; Mitsuhashi, T.; Li, C.; Abe, I. Cytochrome P450 for citreohydrinol synthesis: oxidative derivatization of the andrastin scaffold. *Org. Lett.* **2016**, 18 (2), 296–299.

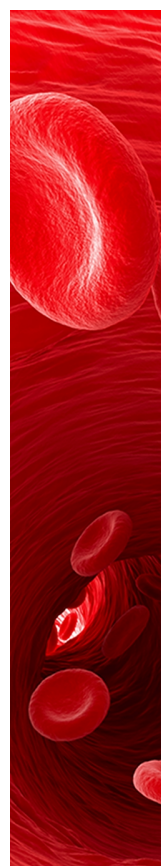
(50) Zhang, X.; Wang, T. T.; Xu, Q. L.; Xiong, Y.; Zhang, L.; Han, H.; Xu, K.; Guo, W. J.; Xu, Q.; Tan, R. X.; Ge, H. M. Genome mining and comparative biosynthesis of meroterpenoids from two phylogenetically distinct fungi. *Angew. Chem., Int. Ed.* **2018**, 57 (27), 8184–8188.

(51) Lv, J. M.; Hu, D.; Gao, H.; Kushiro, T.; Awakawa, T.; Chen, G. D.; Wang, C. X.; Abe, I.; Yao, X. S. Biosynthesis of helvolic acid and identification of an unusual C-4-demethylation process distinct from sterol biosynthesis. *Nat. Commun.* **2017**, 8 (1), 1644.

(52) Ziegler, J.; Facchini, P. J. Alkaloid biosynthesis: metabolism and trafficking. *Annu. Rev. Plant Biol.* **2008**, 59, 735–769.

(53) Shinohara, Y.; Takahashi, S.; Osada, H.; Koyama, Y. Identification of a novel sesquiterpene biosynthetic machinery involved in astellolide biosynthesis. *Sci. Rep.* **2016**, 6 (1), 32865.

(54) Wang, G. Q.; Chen, G. D.; Qin, S. Y.; Hu, D.; Awakawa, T.; Li, S. Y.; Lv, J. M.; Wang, C. X.; Yao, X. S.; Abe, I.; Gao, H. Biosynthetic pathway for furanosteroid demethoxyviridin and identification of an unusual pregnane side-chain cleavage. *Nat. Commun.* **2018**, 9 (1), 1838.



CAS BIOFINDER DISCOVERY PLATFORM™

**CAS BIOFINDER
HELPS YOU FIND
YOUR NEXT
BREAKTHROUGH
FASTER**

Navigate pathways, targets, and
diseases with precision

Explore CAS BioFinder

CAS
A Division of the
American Chemical Society